16

Carbon Speciation and Solubility in Silicate Melts

Natalia Solomatova[1], Razvan Caracas[1,2], and Ronald Cohen[3,4]

ABSTRACT

To improve our understanding of the Earth's global carbon cycle, it is critical to characterize the distribution and storage mechanisms of carbon in silicate melts. Presently, the carbon budget of the deep Earth is not well constrained and is highly model-dependent. In silicate melts of the uppermost mantle, carbon exists predominantly as molecular carbon dioxide and carbonate, whereas at greater depths, carbon forms complex polymerized species. The concentration and speciation of carbon in silicate melts is intimately linked to the melt's composition and affects its physical and dynamic properties. Here we review the results of experiments and calculations on the solubility and speciation of carbon in silicate melts as a function of pressure, temperature, composition, polymerization, water concentration, and oxygen fugacity.

16.1. INTRODUCTION

Evidence of carbon-bearing phases in the Earth's mantle includes the release of CO_2 in volcanic eruptions, dissolved CO_2 in magmatic glasses and glass inclusions (Mörner & Etiope, 2002), diamonds and carbonate minerals in mantle xenoliths (Eggler, 1987; Sobolev & Shatsky, 1990), and the existence of carbonatite and kimberlite magmas (Wyllie et al., 1990). There are two possible sources of carbon:

[1] CNRS, Ecole Normale Supérieure de Lyon, Université de Lyon, Laboratoire de Géologie de Lyon, Lyon, France

[2] CEED, The Center for Earth Evolution and Dynamics, University of Oslo, Oslo, Norway

[3] Extreme Materials Initiative, Carnegie Institution for Science, Washington, DC, USA

[4] Department für Geo- und Umweltwissenschaften, Ludwig Maximilians Universität München, München, Germany

primordial carbon and the carbon delivered by later cometary and asteroid bombardment. Primordial carbon existed in the proto-Earth and subsequently survived the moon-forming impact, and its amount is currently unknown. From all existent carbon, part of it might be locked in the core, part in some deep mantle reservoir, another fraction lies at the surface, and the remaining is resurfaced after surviving subduction. To determine how much carbon may have remained in the Earth after the giant impact, the chemistry and thermodynamics of carbon in silicate (particularly, with the bulk silicate Earth composition) must be determined as a function of pressure and temperature. Estimates of the amount of carbon exchanged between the surface and the mantle range between 30 and 130 megatons per year, and estimates of the carbon concentration stored within the core range between 0.2 and 4 wt.% (McDonough, 2003; Mookherjee et al., 2011; Wood, 1993). Carbon is mainly subducted into the Earth in the form of carbonates within metasomatically calcium-enriched basaltic rock, calcified serpentinites, and sedimentary carbonaceous ooze of the seafloor (Brenker et al.,

2006). Some carbonates may survive subduction by undergoing transitions to denser carbonate phases (Brenker et al., 2006; Isshiki et al., 2004; Mao et al., 2011; Merlini et al., 2012; Oganov et al., 2008; Ono et al., 2005; Solomatova & Asimow, 2017). If a fraction of carbon is subducted into the lower mantle, all possible carbon sinks need to be determined. Due to carbon's low solubility in crystalline silicates (Keppler et al., 2003; Panero & Kabbes, 2008; Shcheka et al., 2006), carbon strongly partitions into silicate melts relative to silicate minerals. This chapter briefly summarizes the experiments and calculations that have been performed on carbon-bearing silicate melts and glasses, particularly the speciation and solubility of carbon as a function of pressure, with a primary goal to expose areas that remain controversial or unknown that would especially benefit from ab initio molecular dynamics simulations. There have been at least three excellent review papers on carbon in silicate melts (see Holloway & Blank, 1994; Ni & Keppler, 2013; Webster et al., 2011), as well as several papers that have done an excellent job summarizing, tabulating, and plotting together data from previous studies (e.g. Duan, 2014; Shishkina et al., 2014). Here, we provide a perspective from computational mineral physics on what is critical to investigate in the near future. Furthermore, we contribute our calculations on carbonated forsterite melts to improve our understanding of diamond formation from silicate melts.

16.2. EXPERIMENTS ON SILICATE MELTS

Experimentally, standard difficulties hinder the in situ analysis of silicate melts: absence of periodicity, which prevents refining structure and density from X-ray diffraction, and high background optical radiation, which hinders spectroscopic measurements. Glasses from quenched melts are amenable to study, but the structure may change and carbon may diffuse during quench. Nevertheless, the carbon content of quenched samples that were equilibrated with other phases (solids, liquids or gases) can be determined using a bulk analyzer, secondary-ion mass spectrometry, nuclear magnetic resonance experiments, and most commonly, Fourier-transform infra-red (FTIR) spectroscopy. FTIR is able to determine both CO_2 and H_2O concentrations with a high level of accuracy if the molar absorptivity is well calibrated against absolute techniques, such as a bulk carbon analyzer. The solubility and speciation of carbon depends on the composition, oxygen fugacity, H_2O and CO_2 concentrations, temperature, pressure, and NBO/T (the ratio between the number of Non-Bridging Oxygen atoms and Tetrahedrally-coordinated cations; this ratio is defined in slightly different ways by different authors, depending on which cations are considered tetrahedrally coordinated).

Experiments have generally been conducted in large-volume presses in the pressure range of 1–4 GPa and temperature range of 1000 °C–2000 °C. Typically, the procedure is to saturate a melt at high pressure and temperature with CO_2 until equilibrium is reached and then rapidly quench the melt to produce a glass that ideally retains the structure of the melt. The examination of carbon speciation has mostly been limited on quantifying the CO_2-to-CO_3^{2-} ratio as a function of composition. Unfortunately, with a few exceptions (e.g. Sen et al., 2013), experimental studies have not pursued the formation of more complex species, such as carbon-carbon polymers, organic molecules, or even silicon-carbon and iron-carbon polymers.

16.2.1. Speciation of Carbon

Experiments have demonstrated that at 1–4 GPa and 1000 °C–2000 °C, the $CO_2/(CO_2+CO_3^{2-})$ ratio is most strongly dependent on the composition of the melt. It has been shown that carbon exists almost exclusively as CO_3^{2-} (rather than CO_2) in mafic melts, such as basalt (Fine & Stolper, 1986; Fogel & Rutherford, 1990; Shishkina et al., 2014; Thibault & Holloway, 1994), olivine melitite (Brey, 1976; Brey & Green, 1976), phono-tephrite (Behrens, 2009), nephelinite (Brooker et al., 1999; Shishkina et al., 2014), and icelandite (Jakobsson, 1997). In the sequence of basalt, andesite, rhyodacite, and rhyolite melts, Fogel and Rutherford (1990) showed a general increase in the CO_2/CO_3^{2-} ratio, such that carbon exists exclusively as CO_2 in rhyolite and as CO_3^{2-} in basalt, while in albite-anorthite melts, Brey (1976) found that the CO_2/CO_3^{2-} ratio increases with increasing albite content. King and Holloway (2002) found that highly polymerized melts with high ionic porosities (>48.3%) and low nonbridging oxygen/tetrahedral oxygen (<0.3) have a higher concentration of molecular CO_2. In melts along the $NaAlO_2$-SiO_2 join (from $NaAlSi_6O_{14}$ rhyolite rock composition to pure $NaAlSiO_4$ nepheline), Brooker et al. (1999) found that the relative and absolute abundance of CO_3^{2-} increases with increasing $NaAlO_2/SiO_2$ at the expense of CO_2, such that carbon in $NaAlSiO_4$ exists almost exclusively as CO_3^{2-}, whereas carbon in $NaAlSi_6O_{14}$ exists almost exclusively as CO_2. The total solubility of carbon decreases as $NaAlO_2$ is added to SiO_2, up to a $NaAlO_2/SiO_2$ ratio of about 0.5, after which the trend reverses and there is a sharp increase in the solubility of carbon. The CO_2/CO_3^{2-} ratio decreases with increasing pressure at constant temperature (in other words, carbon increases coordination with pressure). The effect of temperature is subtler: at constant pressure, the CO_3^{2-} concentration decreases with increasing temperature between 1450 °C and 1600 °C and increases with increasing temperature from 1600 °C to 1700 °C, in agreement with

the results of Fine and Stolper (1985). Konschak and Keppler (2014) examined the speciation of carbon in dacite, phonolite, basaltic andesite, and alkali silicate melts using synchrotron infrared spectroscopy and diamond anvil cells up to 1000 °C and 200 kbar, finding a correlation between NBO/T and speciation. In alkali silicate and basaltic andesite, carbon exists exclusively as carbonate, while in dacite and phonolite, carbon exists as a mixture of CO_2 and CO_3^{2-}. With increasing temperature, the effect of composition on carbon's speciation decreases as carbon shifts from existing as CO_3^{2-} to CO_2. They find that the speciation of carbon is largely insensitive to pressure up to 200 kbar, and that composition and temperature have a much stronger effect.

The speciation of carbon in highly reduced melts is poorly understood. Whereas Morizet et al. (2010) suggested that applying reducing conditions would not affect carbon speciation in hydrous melts, Kadik (2004) observed that carbon is dissolved primarily as atomic carbon in reduced ferrobasalt. Kadik observed direct Si-C bonds in ferrobasaltic glass using Raman spectroscopy, and Sen et al. (2013) observed that carbon exclusively bonds to silicon rather than oxygen in a reduced SiLiOC melt using nuclear magnetic resonance experiments, giving rise to their contrary conclusions. Although it is typically expected that in shallow melts carbon will bond to oxygen to form CO_2 or CO_3^{2-}, it is possible that in more reduced melts and especially at higher pressures, carbon will bond directly to silicon instead of oxygen. See the computational section for theoretical evidence of Si-C bonds in pyrolitic melt. Additional experiments and specific measurements are needed to constrain the speciation of carbon in reduced silicate melts. In summary, at lithospheric conditions, i.e. within the pressure range of 0.5–4 GPa and at temperatures below 2000 °C, the CO_2/$(CO_2+CO_3^{2-})$ ratio is most strongly affected by the composition, and in particular, the silica content of the melt (Figure 16.1). Carbon exists almost exclusively as CO_2 in silica-rich felsic melts (e.g., rhyolite) and as CO_3^{2-} in silica-poor mafic melts (e.g., basalt, olivine melitite and nepheline melts). The CO_2/$(CO_2+CO_3^{2-})$ ratio is also negatively correlated with pressure and generally insensitive to temperature; there remain disagreement and insufficient data on the effect of the H_2O content on the speciation of carbon. Additional studies are needed to refine the effect of temperature, H_2O content, and NBO/T, as well as the effect of network-modifying cations within the melt.

16.2.2. Solubility of Carbon

The solubility of carbon within a silicate melt depends most strongly on pressure and composition. The effects of temperature, water content, and oxidation state are
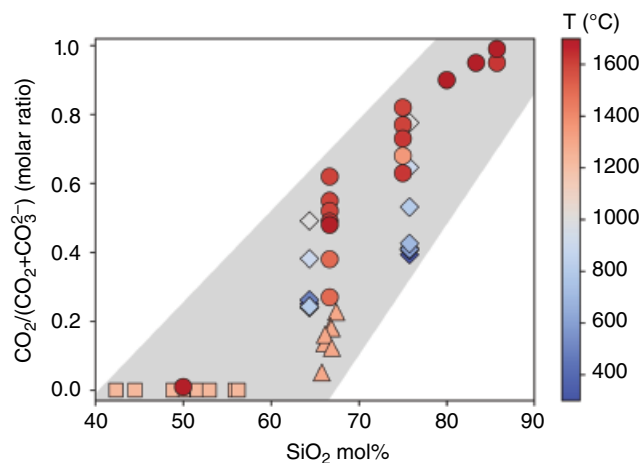
Figure 16.1 Molar ratio, CO_2/$(CO_2+CO_3^{2-})$ as a function of silica content at 300 °C–1700 °C for melts and glasses along the $NaAlO_2$-SiO_2 join from Brooker et al. (1999) (circles), andesite melts from King and Holloway (2002) (triangles), phonolite and dacite melts from Konschak and Keppler (2014) (diamonds), and mafic melts from Shishkina et al. (2014) (squares). The data from Brooker et al. (1999) and King and Holloway (2002) were obtained at 1–2 GPa and 1 GPa, respectively. Shishkina et al. (2014) did not observe any molecular CO_2 species for the range of mafic melts investigated at 1200 °C–1250 °C up to 0.5 GPa. Konschak and Keppler (2014) reported that the carbon speciation is independent of pressure in the pressure range of 3–20 GPa at temperatures of up to 1000 °C; however, Brooker et al. (1999) observed a negative correlation of CO_2/$(CO_2+CO_3^{2-})$ and pressure. In either case, the effect of pressure and temperature is secondary to the effect of silica content on carbon's speciation. See electronic version for color representation of the figures in this book.

less well defined at the present time, due to discrepancies in the literature. Solubility can be difficult to measure accurately due to several factors. Hydrogen and carbon may diffuse into the silicate melt, or small amounts of melt components may dissolve into the fluid phase, affecting the measured carbon solubility. The oxidation state may change due to the capsule material, resulting in changes in carbon speciation, and thus, solubility. Furthermore, the use of different molar absorptivity standards for the CO_2 and CO_3^{2-} for the FTIR bands may be a source of inconsistencies in reported solubilities. Here we summarize the current data on carbon solubility in a variety of silicate melt compositions, highlighting the need for additional high-quality experiments to resolve discrepancies and gaps in the literature. We use the term *carbon solubility* to encompass the cumulative solubility of CO_2 and CO_3^{2-}, making the distinction when necessary.

There is good agreement within the experimental literature that carbon solubility in silicate melts increases rapidly with increasing pressure (Behrens et al., 2004; Blank,

1993; Botcharnikov et al., 2005; Botcharnikov et al., 2007; Brooker et al., 1999; Fogel & Rutherford, 1990; Jendrzejewski et al., 1997; Shishkina et al., 2014). For example, in rhyolitic melts at 1123–1323 K, CO_2 solubility increases from roughly 120 ppm at 20 MPa to 800–1000 ppm at 140 MPa to 3700 ppm at 660 MPa (Blank, 1993; Fogel & Rutherford, 1990). In dacitic melts, the maximum CO_2 solubility increases from 800 ppm at 100 MPa to 3000 ppm at 500 MPa (Behrens et al., 2004), and in andesitic melts, the CO_2 solubility increases from 175 ppm at 50 MPa to 3300 ppm at 500 MPa (Botcharnikov et al., 2005). Similarly, in shoshonitic melts, Vetere et al. (2011) found that the concentration of CO_2 (in the form of carbonate) increased from 307 ppm at 50 MPa to 2932 ppm at 400 MPa. Thus, there is a consensus that more carbon species can dissolve in silicate melts with increasing pressure, and thus with increasing depth. There is also a strong dependence of the carbon solubility on the composition of the silicate melts, most notably affected by the degree of polymerization (Brooker et al., 2001a; Brooker et al., 2001b; Mysen et al., 2009; Shishkina et al., 2014) and concentration of CaO (Brey, 1976; Holloway, 1976; Iacono-Marziano et al., 2012; King & Holloway, 2002; Moore, 2008; Papale et al., 2006; Shishkina et al., 2014). Holloway (1976) observed that carbon solubility is positively correlated with the Ca/(Ca+Mg) ratio. Brey (1976) found that the solubility of carbon in olivine melilite (8.3–9.5 wt.% CO_2) is much higher than in albite-anorthite (1.6–2.5 wt.% CO_2), for which the solubility increases slightly with increasing anorthite content. Brooker et al. (2001a, 2001b) observed a negative correlation with MgO content and a positive correlation with NBO/T. King and Holloway (2002) found that carbon solubility is negatively correlated with the Si+Al mole fraction and positively correlated with cations that have a large Gibbs free energy of decarbonation or a high charge-to-radius ratio (e.g. Ca). Alkalis have also been found to have a positive correlation with the solubility of CO_2 (Behrens et al., 2009; Lesne et al., 2011; Vetere et al., 2014), although the relationship is more complex. Shishkina et al. (2014) found that at 500 MPa and the H_2O content extrapolated to 0 wt.%, the CO_2 concentration increases from tholeiite (~3400 ppm) to alkali basalt (~5200 ppm), to basanite (~7400 ppm), to phonotephrite (~8500 ppm), to nephelinite (~14000 ppm). To describe the complex relationship between composition and carbon solubility, Shishkina et al. formulated a modified Π parameter (originally proposed by Dixon, 1997, for a limited range of silica contents) using eight compositions of silicate melt combined with previous data sets. The Π parameter in Shishkina et al. is defined as the ratio between the freely diffusing cations and the tetrahedral network, $(Ca^{2+} + 0.8K^+ + 0.7Na^+ + 0.4Mg^{2+} + 0.4Fe^{2+})/(Si^{4+} + Al^{3+})$, as reflecting the degree of polymerization of the melt. The relationship between the natural log of the solubility of CO_2 and Π was found to be $1.167*lnP + 0.671* \Pi + 0.65$ (where P is pressure), obtained from the linear regression of 48 values of CO_2 solubilities at 50–500 MPa. The newly formulated Π parameter in Shishkina et al. is the most rigorous parameterization of the compositional effect on carbon solubility at the present time.

Although most studies demonstrate a negative correlation between total carbon solubility and H_2O content (Behrens et al., 2004; Blank et al., 1993; Botcharnikov et al., 2005; Botcharnikov et al., 2006; Fogel & Rutherford, 1990; Mattey, 1991; Moussallam et al., 2016; Pan et al., 1991; Pawley et al., 1992; Shishkina et al., 2010; Stolper & Holloway, 1988; Tamic et al., 2001), several studies observed a positive correlation (Behrens et al., 2004; Behrens et al., 2009; Iacono-Marziano et al., 2012; King & Holloway, 2002; Jakobssen, 1997). Below about 2×10^4 ppm H_2O, there is generally a weak correlation between the H_2O and CO_2 concentrations, while at higher H_2O concentration the CO_2 solubilities tend to drop (Ni & Keppler, 2013). For example, at 2 kbar and 1250–1300 °C, the CO_2 solubility in basaltic and rhyolitic melts plateaus around 1000 ppm CO_2 up to around 2×10^4 ppm H_2O, gradually dropping to 0 ppm CO_2 by 5×10^4 ppm H_2O in basaltic melt (Botcharnikov et al., 2005; Shishkina et al., 2010) and by 5.6×10^4 ppm H_2O in rhyolitic melt (Tamic et al., 2001). On the other hand, King and Holloway (2002) observed a total CO_2 solubility increase by about 0.06 wt.% per wt.% of H_2O in andesite glass at 10 kbar and 1300 C: as the H_2O concentration increased from 0 to 3.4 wt.%, molecular CO_2 decreased from 0.07 to 0.01 wt.% and CO_3^{2-} increased from 0.25 to 0.57 wt.%. Iacono-Marziano et al. (2012) hypothesized that a positive correlation between CO_2 and H_2O concentrations may be due to NBO formation, which promotes CO_3^{2-} formation, thus increasing the total carbon solubility. The solubility data of icelandite from Jakobssen (1997) shows no trend with H_2O when plotted against dissolved CO_2 (Ni & Keppler, 2013), whereas there is a positive trend when plotted against dissolved CO_2 normalized to the CO_2 partial pressure. Nevertheless, the majority of studies see a negative correlation and it is not clear at the present time what is responsible for the discrepancy in these studies.

The effect of temperature on the solubility of carbon is also poorly constrained. Generally, carbon solubility seems to be weakly dependent on temperature, such that the sign of the trend depends on the composition. For example, it has been shown that carbon solubility decreases weakly with increasing temperature for albitic melts (Blank & Brooker, 1994; Brooker et al., 1999; Stolper et al., 1987) and decreases strongly for rhyolitic melts at 0.1 GPa (Blank, 1993; Fogel & Rutherford, 1990; Ni & Keppler, 2013). Eitel and Weyl (1932) observed a

negative dependence in sodium metasilicate melts at 750 atm, and Pearce (1964) observed pronounced negative temperature dependence in Na_2O-SiO_2 melts at 1 atm. However, Brooker et al. (1999) observed a slight increase in solubility with increasing temperature for $NaAlSiO_4$ and no dependence for melts with compositions between $NaAlSi_4O_{10}$ and $NaAlSi_6O_{14}$. In more mafic compositions, there is even less consensus. Brey and Green (1976) observed a slight negative relationship in olivine melilitite at 3 GPa with 9% CO_2 dissolved at 1450 °C, 8.5% at 1550 °C, and 8.3% at 1650 °C, while Mysen et al. (1976) observed a strong positive correlation with temperature at 1400–1700C above 1 GPa. Pan et al. (1991) demonstrated that carbon solubility is temperature-independent in tholeiitic basalt melt at 1–1.5 GPa and 1300 °C–1600 °C. It is possible that there are discrepancies in the effect of temperature due to different quenching methods and/or quality of the glass as an analog for certain compositions. In any case, additional studies are needed to constrain the effect of temperature on carbon solubility. At least at uppermost mantle pressures and temperatures, increasing oxygen fugacity increases the solubilities of carbon and hydrogen (Kadik, 2004; Morizet et al., 2010; Stanley et al., 2011). Morizet et al. (2010) found a strong positive correlation between carbon solubility and oxidation state in haploblastic glasses at 1250 °C and 200–300 MPa, finding that the CO_2 content changes from 680 to 1320 ppm between $\Delta FMQ - 2.6$ and $\Delta FMQ + 2.6$ independently of H_2O content changing from 1.3 to 4.0 wt.%. Stanley et al. (2011) found that the CO_2 content increases from 51 ppm at IW to 510 ppm at IW + 1 in a synthetic melt based on the Adirondack-class Humphrey basalt, at 1–2.5 GPa and 1400 °C–1625 °C. At greater depths, however, the relationship between oxygen fugacity and carbon solubility is unknown. It has been hypothesized that carbon may behave like oxygen in reduced high-pressure melts (Sen et al., 2013) and possibly result in an increase in solubility.

16.3. SIMULATIONS OF SILICATE MELTS

It remains a great challenge to experimentally measure the structural properties of melts at simultaneously high pressures and temperatures. The majority of experiments require quenching of the melt prior to analysis, which may change the local structure and coordination environment of the atoms, as well as the volatile concentration (Behrens & Nowak, 2003; Brey, 1976; Guillot & Sator, 2011). Additionally, experiments on carbon solubility and speciation in silicate melts have mostly been limited to pressures of up to 4 GPa and temperatures of up to 2000 °C, while calculations can determine the precise behavior of atoms and directly calculate thermodynamic properties at a wide range of pressures and temperatures.

On the other hand, the atomistic simulations have strong size limitations, as they typically contain a few hundred atoms in a periodically repeated simulation box. This may be somewhat mitigated by long simulation times and large number of configurations, in a push to cover as much as possible from the configurational space.

Molecular dynamics calculations can be performed with classical or ab initio methods. In classical molecular dynamics, the forces between atoms are calculated from empirical interatomic potentials, whereas in ab initio molecular dynamics, forces are determined from electronic structure calculations (e.g. with density functional theory). In both cases, the motions of the atoms are calculated with Newton's second law and are treated classically. Due to computational expense, ab initio molecular dynamics are limited by the number of atoms and duration of the simulation; the latter can be orders of magnitude higher than for classical molecular dynamics. The level of accuracy of classical molecular dynamics depends on the quality of the parametrization of the interatomic potentials, which depends on the accuracy of the reference data. Furthermore, extrapolation to pressure-temperature conditions beyond the conditions of the reference data decreases the accuracy of the potentials. Although ab initio molecular dynamics depends on several approximations (e.g., the exchange-correlation energy and the treatment of core electrons), it is based on first principles in the sense that it does not require parameterization with experimental data. For the case of high-pressure, high-temperature silicate melts, the reference data is scarce or nonexistent, especially within the large range of pressure and temperature conditions of planetary interiors, and so ab initio methods are presumably more reliable. For example, Vuilleumier et al. (2015) found that their classical simulations were not sufficiently viscous, as the atomic diffusion coefficients were larger than experimental values. They also found disagreement in the CO_2 concentration as a function of composition when comparing their results from classical simulations to ab initio simulations, concluding that the empirical force fields need to be improved. Furthermore, the ratio of CO_2 to CO_3 is severely overestimated with classical molecular dynamics in the calculations of Guillot and Sator (2011) (see section 3.2). Thus, even though empirical methods allow for a larger number of atoms and longer simulation duration, experimental results on carbon speciation are far better reproduced with ab initio methods. The effect of cell size (i.e., number of atoms) on carbon speciation in ab initio molecular dynamics simulations is not currently well understood.

Thus far, there have been five studies on carbonated silicate melts using molecular dynamics simulations. The two first studies were conducted at pressure and temperature conditions of the upper mantle: Guillot and Sator

(2011) implemented classical molecular dynamics to quantify the solubility of carbon in rhyolite, MORB, and kimberlite melts at 2–15 GPa and 1473–2273 K; and Vuilleumier et al. (2015) used a combination of classical and ab initio molecular dynamics to study the speciation of carbon in basaltic and kimberlitic melts with ~20 wt.% CO_2 at 2073 K and 12 GPa. Subsequently, simulations at lower mantle pressures and temperatures were conducted. Ghosh et al. (2017) used ab initio molecular dynamics to examine the speciation of carbon in $MgSiO_3$ melt with 5–16 wt.% CO_2 at 2200–6000 K and 140 GPa, while Ghosh and Karki (2017) examined the transport properties of $MgSiO_3$ melt with 16.1 wt.% CO_2 at 2200–5000 K up to 140 GPa. Most recently, Solomatova et al. (2019) used ab initio molecular dynamics to examine the speciation and polymerization of carbon in pyrolite melt with 5–10 wt.% CO_2 at 3000–5000 K up to 140 GPa. The compositions and carbon concentrations of the ab initio molecular dynamics simulations are summarized in Table 16.1.

In this chapter, we add our simulations on pure and carbonated Mg_2SiO_4 forsterite melt at 3000 K and up to 120 GPa. We have worked on several distinct compositions: Mg_2SiO_4, Mg_2SiO_4+C, Mg_2SiO_4+CO_2, and Mg_2SiO_4+$MgCO_3$, and study the effect of carbonation on the melt properties as well as the differences between the various carbon species. We have employed the Qbox package (Gygi, 2018). We start the calculations with solid Mg_2SiO_4 forsterite. Forsterite, the Mg-end member term of the mineral olivine, has an orthorhombic structure with 4 formula units per unit cell, namely 28 atoms. We consider a 2x1x2 supercell containing 112 atoms. After static structural relaxation, we perform a molecular-dynamics calculation on the solid, raising the temperature well above the melting point. Once we reach melting,

we decrease the temperature and thermalize the melt at the desired value closer to realistic telluric conditions. Here, we performed a high-pressure study along the 3000 K isotherm. All simulations are NVT type, meaning the Number of particles, the Volume of the simulation box, and the Temperature are kept constant. This is numerically simpler than the NPT ensemble, where pressure instead of volume is fixed. Temperature is controlled via a Nose-Hoover thermostat, and the time step of the simulations is 0.75 fs. Temperature is monitored throughout the simulations to maintain fluctuations within a couple hundred degrees above and below the average 3000 K. We compute the electronic density and wave functions sampling the Brillouin zone in the reciprocal space using only the Γ point. We add carbon in the silicate melt as C atoms, CO_2 molecules, or $MgCO_3$ groups. The addition of the supplementary atoms is done in the interstitial pores of the melt at low pressure. CO_2 is added as a linear molecule, and $MgCO_3$ as a Mg cation about 2 Å apart on top of a CO_3 triangular anionic group. The new melts are first thermalized for one full picosecond in order to dissipate the interatomic forces and equilibrate the strains and then compressed along the 3000 K isotherm up to lower-mantle pressures.

16.3.1. Solubility of Carbon Dioxide in the Silicate Melt

Guillot and Sator (2011) observed a strong positive correlation of carbon solubility with pressure. For example, at 1673 K, carbon solubility in a basaltic melt increased from 2 wt.% CO_2 at 2 GPa to 30 wt.% CO_2 at 10 GPa. A weak negative correlation with temperature was observed and the effect of temperature increases with increasing pressure, such that at 2 GPa, there is almost no

Table 16.1 Carbon concentrations in the simulated melts using ab initio molecular dynamics, expressed as the formula units of carbon species added, wt.% of carbon species added, wt.% of C and mol% of C. The chosen carbon concentrations of 1.4–4.7 wt.% C reflect the range of carbon present in carbonaceous chondrites (0–6 wt.% C) (Pearson et al., 2006), which are regarded as the building blocks of our planet.

Composition, Supercell Formula	Reference	Carbon Species Added	wt.% of Carbon Species Added	wt.% C	mol% C
Enstatite, $32MgSiO_3$	Ghosh et al. (2017)	4 CO	3.37 wt.% CO	1.45	2.38
		4 CO_2	5.20 wt.% CO_2	1.42	2.33
		14 CO	10.88 wt.% CO	4.66	7.45
		14 CO_2	16.09 wt.% CO_2	4.39	6.93
Pyrolite, $NaCa_2Fe_4Mg_{30}Al_3Si_{24}O_{89}$	Solomatova et al. (2019)	4 CO	3.35 wt.% CO	1.44	2.48
		4 CO_2	5.16 wt.% CO_2	1.41	2.42
		8 CO	6.48 wt.% CO	2.78	4.97
		8 CO_2	9.82 wt.% CO_2	2.68	4.52
Forsterite, $16Mg_2SiO_4$	This study	8 C	4.09 wt.% C	4.09	6.67
		4 CO_2	7.25 wt.% CO_2	1.98	3.23
		8 CO_2	13.52 wt.% CO_2	3.69	5.88
		4 $MgCO_3$	13.03 wt.% $MgCO_3$	1.86	3.03

difference in solubility with temperature, whereas at 5 GPa, the solubility of CO_2 decreases from 10 wt.% at 1673 K to 7 wt.% at 2273 K. At low pressure, they demonstrate excellent agreement with experiments (Hammouda, 2003; Mattey, 1991; Pan et al., 1991; Thomsen & Schmidt, 2008). For example, both Guillot and Sator (2011) and Mattey (1991) predict CO_2 solubility in basaltic melt of 1.5 wt.% at 2 GPa and 1673 K. At 3.5 GPa and 1573 K, Thomsen and Schmidt (2008) report a CO_2 solubility of 5 wt.% CO_2 in a complex carbonatite melt, similar to the value of 6 wt.% CO_2 at 3.5 GPa and 1673 K predicted by Guillot and Sator (2011). The solubility is also weakly correlated with silica content, only becoming noticeable above about 10 GPa. The solubility of CO_2 at 10 GPa and 2273 K is about 25 wt.% in basalt and 24 wt.% in rhyolite, while at 15 GPa and 2273 K, the solubility of CO_2 is about 37 wt.% in basalt and 34 wt.% in rhyolite. Although Guillot and Sator (2011) predict excellent agreement of solubility with experiments, the form in which carbon exists (CO_2 vs. CO_3^{2-}) is significantly different than experimental observations (see below).

16.3.2. Carbon Coordinated by Oxygen

Guillot and Sator (2011) found that the proportion of CO_3^{2-} increases with increasing pressure and decreases with increasing temperature relative to CO_2. Although experiments on quenched mafic melts have shown that carbon exists exclusively as CO_3^{2-} (e.g. Fogel & Rutherford, 1990; Shishkina et al., 2014; Thibault & Holloway, 1994),

Guillot and Sator predicted a significant CO_2 content ($CO_2/[CO_2+CO_3^{2-}]\sim0.6$ at 1873 K), noting that a low-temperature extrapolation to 300 K would agree with the experimental results, implying that the speciation (and thus, solubility) of carbon in the recovered silicate glasses (i.e. quenched silicate melt) is not an accurate representation of the high-temperature silicate melt. The implication is that the experimental results on carbon-bearing silicate glasses are unreliable. However, when the $CO_2/(CO_2+CO_3^{2-})$ ratio is plotted for the computational studies on carbon-bearing $MgSiO_3$ (Ghosh et al., 2017) and carbon-bearing pyrolite (Solomatova et al., 2019), the concentrations of CO_2 are substantially lower than in Guillot and Sator (2011) at comparable temperatures (Figure 16.2). For example, at 2–3 GPa, Ghosh et al. (2017) observed 1%–4% $CO_2/(CO_2+CO_3^{2-})$ at 2200 K in $MgSiO_3$, but Guillot and Sator (2011) observed 70% $CO_2/(CO_2+CO_3^{2-})$ at 2273 K in MORB. The discrepancy between the computational studies may be best explained by the difference in methodology. Guillot and Sator (2011) used classical molecular dynamics on a CO_2 saturated composition (~25 wt.% CO_2 at 10 GPa), but Ghosh et al. (2017) and Solomatova et al. (2019) used ab initio molecular dynamics on melts with 5–16 wt.% CO_2. Vuilleumier et al. (2015) used a combination of classical and ab initio molecular dynamics to study the speciation of carbon in basaltic and kimberlitic melts with ~20 wt.% CO_2 at 2073 K and 12 GPa, finding that most of the carbon exists as CO_3^{2-}. With ab initio molecular dynamics, the $CO_2/(CO_2+CO_3^{2-})$ ratio is 0.15 for the basaltic melt and 0.03
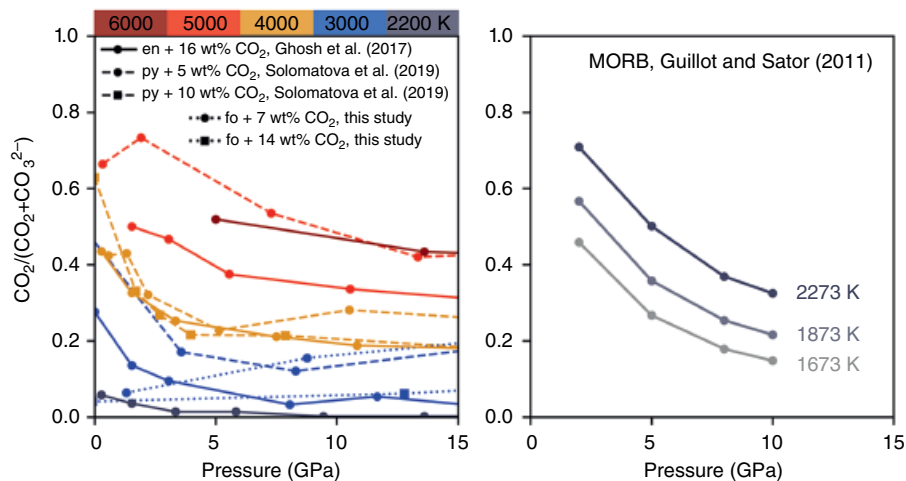
Figure 16.2 Molar ratio, $CO_2/(CO_2+CO_3^{2-})$, as a function of pressure and temperature. Guillot and Sator (2011) predict significantly more CO_2 relative to CO_3^{2-} in MORB melt than Ghosh et al. (2017), Solomatova et al. (2019), and this study in enstatite melt (en), pyrolite melt (py), and forsterite melt (fo), if an extrapolation to lower temperatures is made. In fact, the high $CO_2/(CO_2+CO_3^{2-})$ ratios predicted by Guillot and Sator (2011) at 2273 K are only achieved at 5000 K in Ghosh et al. (2017) and Solomatova et al. (2019). Experiments on basaltic melts at 1–4 GPa and 1000–2200 K observe no CO_2 (Fine & Stolper, 1986; Fogel & Rutherford, 1990; Shishkina et al., 2014; Thibault & Holloway, 1994), in agreement with Ghosh et al. (2017) and in disagreement with Guillot and Sator (2011). See electronic version for color representation of the figures in this book.

for the kimberlitic melt, but with classical molecular dynamics, the ratio is approximately 0.2 for both melts, higher than what is predicted with classical molecular dynamics. At similar conditions (~10–15 GPa and 2200 K), Ghosh et al. (2017) observed essentially no CO_2 in $MgSiO_3$ melt, similar to the results of Vuilleumier et al. (2015) for kimberlitic melt with ab initio molecular dynamics.

In carbonated forsterite melts, the fate of carbon depends on its entry state in the system and, consequently, on the oxidation state of the melt. The general tendency is that the coordination of carbon by oxygen increases with increasing pressure. In forsterite melt with carbon species added as CO_2 and $MgCO_3$, carbon exists almost exclusively in the form of CO_3^{2-} and increases in coordination to CO_4^{4-} with increasing pressure such that carbon in the melt is mostly CO_4^{4-} at core-mantle boundary pressures. In forsterite with reduced carbon added, carbon exists as a mixture of C, CO, and CO_2; with increasing pressure, carbon increases coordination to CO_3^{2-}. At lower-mantle pressures, carbon in the reduced forsterite melt exists as an approximately even mixture of CO, CO_2, and CO_3^{2-} with no CO_4^{4-}. The relative proportions of CO_2, CO_3^{2-}, and CO_4^{4-} are similar at all mantle pressures regardless of the melt chemistry (pyrolite, enstatite, or forsterite), as demonstrated in Figure 16.3.

16.3.3. Carbon Complexes

Although at ambient pressure carbon exists in silicate melts exclusively in unpolymerized forms (e.g. CO, CO_2, and CO_3^{2-}), with increasing pressure it becomes increasingly polymerized (i.e. a higher fraction of carbon atoms are bonded to other carbon atoms) and the carbon species increasingly complex (Ghosh et al., 2017; Solomatova et al., 2019). For example, in pyrolite with 3.35 wt.% CO, nearly none of the carbon is polymerized while at 0 GPa, whereas most of the polymerized carbon exists in C_2O, C_2O_2, and C_2O_3 molecules at ~60 GPa and predominantly as C_2O_{2-6} and C_3O_{4-6} molecules at ~115 GPa and 4000 K (Solomatova et al., 2019). At 12 GPa and 2073 K, Vuilleumier et al. (2015) observed that about 3.7% of all carbon species in basalt + 20 wt.% CO_2 are C_2O_5, which means that 7% of carbon atoms are bonded to another carbon atom, similar to pyrolite + 9.82 wt.% CO_2, in which 5% of carbon is polymerized (Solomatova et al., 2019), and $MgSiO_3$ + 16.1 wt.%, in which 7% of carbon is polymerized (Ghosh et al., 2017), at an equivalent pressure and 4000 K (Figure 16.3).

The polymerization of carbon is inversely dependent on temperature because of the increase in entropy with decreasing polymerization. At 3000 K and 20 GPa, pyrolite with 3.35 wt.% CO has 45% of its carbon polymerized, whereas at 5000 K only about 3% of its carbon
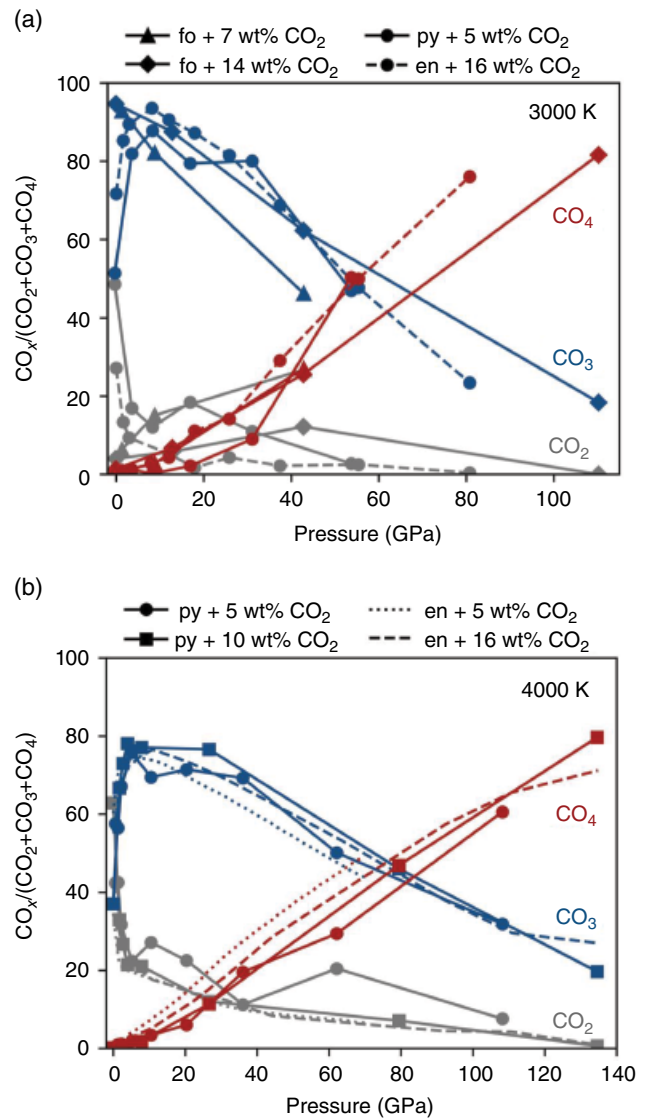

Figure 16.3 Molar ratio, $CO_x/(CO_2+CO_3^{2-}+CO_4^{4-})$ at 3000 K (a) and 4000 K (b) for enstatite (en; Ghosh et al., 2017), pyrolite (py; Solomatova et al., 2019) and forsterite (fo; this study) melts with carbon added into the melt as CO_2. See electronic version for color representation of the figures in this book.

is polymerized (Figure 16.4; Solomatova et al., 2019). In addition to the carbon-carbon polymerization, the degree of clustering between carbon atoms and other cations (predominantly, iron and silicon) also increases with increasing pressure (Figure 16.4). The predisposition of carbon to bond directly to iron suggests that carbon would follow iron during segregation of an iron-rich metallic liquid during core formation in the early Earth, both prior to and after the moon-forming impact.

The oxidation state of the melt has a significant effect on the types of species present (Ghosh et al., 2017; Solomatova et al., 2019). For example, the abundance of
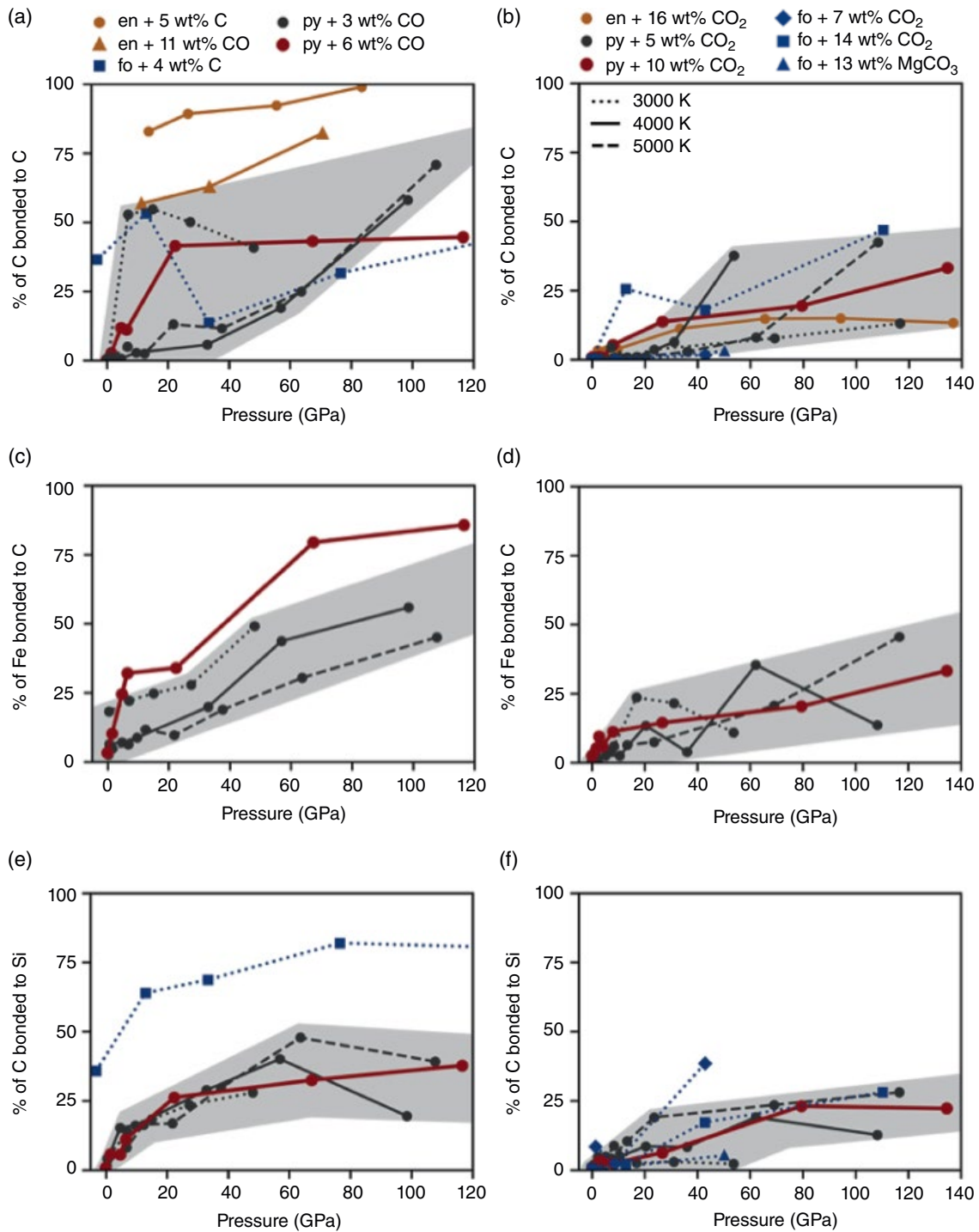
Figure 16.4 Formation of carbon complexes as a function of pressure in simulations on enstatite melt (en; Ghosh et al., 2017); pyrolite melt (py; Solomatova et al., 2019) and forsterite melt (fo; this study) at 3000 K (dotted lines), 4000 K (solid lines), and 5000 K (dashed lines). Left column (a, c, e) includes melts with more reduced carbon species (C and CO); right column (b, d, f) includes melts with more oxidized species (CO_2 and $MgCO_3$). Gray regions mark pyrolite with 3 wt.% CO (left column) and pyrolite with 5 wt.% CO_2 (right column). The degree of carbon-carbon, carbon-iron, and carbon-silicon polymerization generally increases with increasing pressure and decreasing oxidation state of the melts. See electronic version for color representation of the figures in this book.

carbonate ions relative to molecular carbon dioxide is positively correlated to oxygen fugacity. More oxidized pyrolitic melts only contain C_2O_4, C_2O_5, C_2O_6, and C_2O_7, with nearly no C_3O_x species forming while the more reduced melts have a wide range of C_xO_y species present. The oxygen fugacity of the melt is negatively correlated with the degree of carbon-carbon polymerization, as well as the degree of direct carbon-iron and carbon-silicon bonding. Thus, more carbon will bond to other carbon atoms and other cations, such as iron and silicon, in a more reducing environment. Indeed, as Figure 16.4 shows, there is a considerably larger amount of direct carbon-iron bonds for the pyrolite + CO compositions than for the pyrolite + CO_2 compositions. The same is true, and maybe even more pronounced, for the carbon-silicon bonds in case of the forsterite + C compared to forsterite + CO_2. The pyrolite + CO_2 and forsterite + CO_2 show similar behavior, suggesting once more that the oxygen fugacity and/or the state of entry of C into the system are the dominant factors determining its speciation. These findings are in agreement with experimental studies that observed direct carbon-silicon bonds in reduced ferrobasalt melt (Kadik, 2004) and reduced SiLiOC melt (Sen et al., 2013).

16.3.4. Elemental Diffusivities

Ghosh and Karki (2017) examined the transport properties of $MgSiO_3$ enstatite melt with 16.1 wt.% CO_2 at 2200–5000 K up to 140 GPa and found that the addition of carbon increases the diffusivity rates of all elements. However, the diffusivity rates of cations in more complex melts, such as basalt and kimberlite at 12 GPa and 1273 K (Vuilleumier et al., 2015) and pyrolite up to 140 GPa and 3000–5000 K, appear to be unaffected by the presence of carbon (Figure 16.5). The diffusion rates of oxygen and magnesium are nearly identical in carbonated pyrolite and carbonated enstatite, while silicon and carbon appear to have higher diffusion rates in carbonated pyrolite than in carbonated enstatite, indicating that as network formers, silicon and carbon are more mobile in the less polymerized pyrolite melt relative to the more polymerized enstatite melt. There is good agreement in the change of slope of the elemental diffusivities with pressure at around 5 GPa and 4000 K in the different melts. At 3000 K, the diffusion rates of magnesium, silicon, carbon, and oxygen increase with decreasing polymerization of the melt: enstatite < pyrolite < forsterite
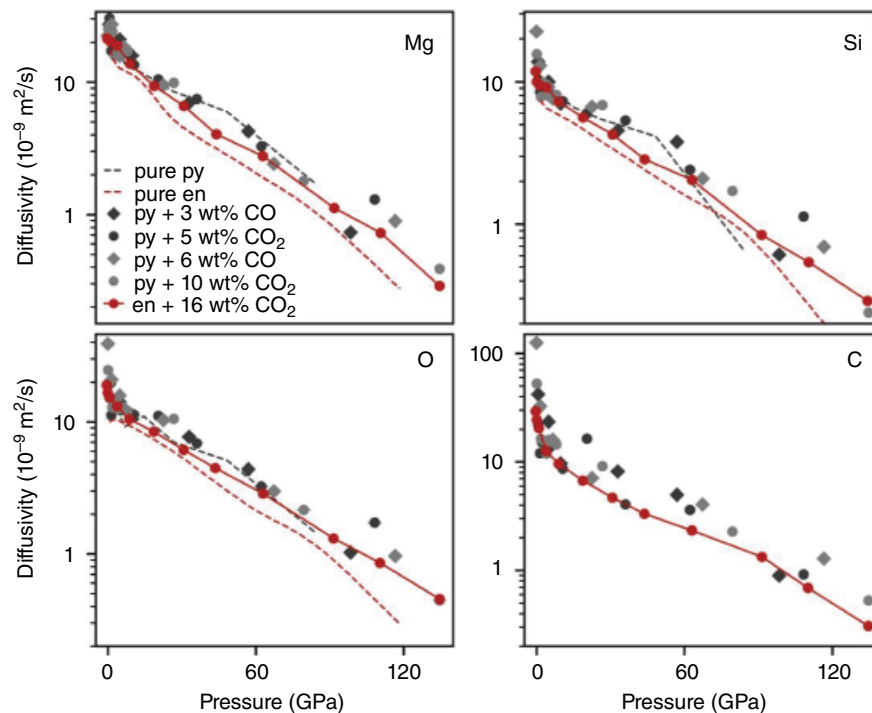
Figure 16.5 Elemental diffusivities of magnesium, silicon, oxygen and carbon at 4000 K in pure pyrolite melt ("pure py"), pure enstatite melt ("pure en"), pyrolite melt with 3.35 wt.% CO ("py + 3 wt.% CO"), pyrolite melt with 5.16 wt.% CO_2 ("pyr + 5 wt.% CO_2"), pyrolite melt with 6.48 wt.% CO ("py + 6 wt.% CO"), pyrolite melt with 9.82 wt.% CO_2 ("py + 10 wt.% CO_2"), and enstatite melt melt with 16.1 wt.% CO_2 ("en + 16 wt.% CO_2"). Pyrolite data is from Solomatova et al. (2019) and enstatite data is from Ghosh and Karki (2017). See electronic version for color representation of the figures in this book.
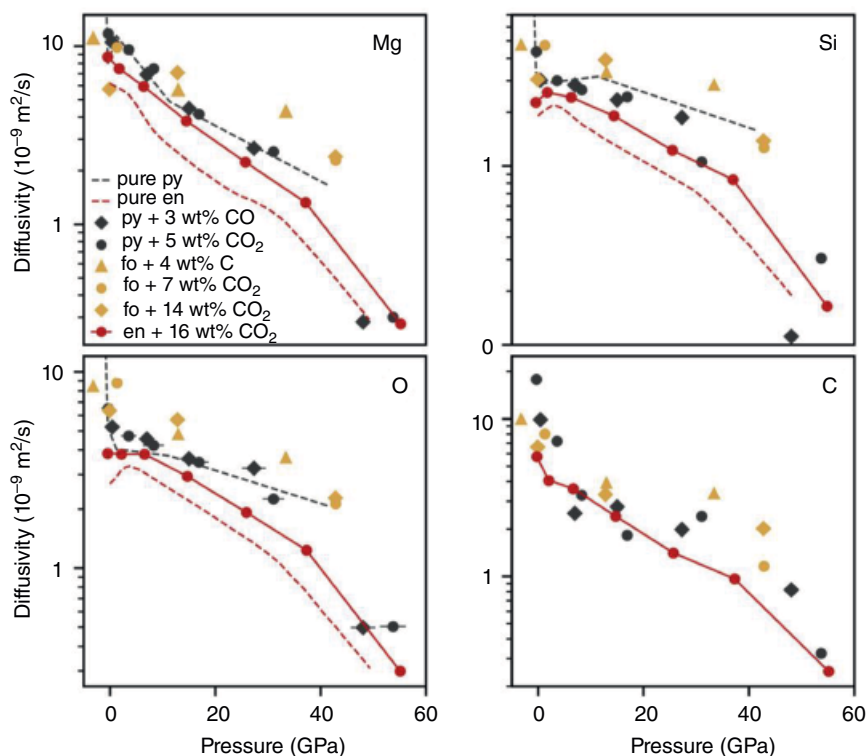
Figure 16.6 Elemental diffusivities of magnesium, silicon, oxygen, and carbon at 3000 K in pure pyrolite melt ("pure py"), pure enstatite melt ("pure en"), pyrolite melt with 3.35 wt.% CO ("py + 3 wt.% CO"), pyrolite melt with 5.16 wt.% CO_2 ("py + 5 wt.% CO_2"), forsterite melt with 4.09 wt.% C ("fo + 4 wt.% C"), forsterite melt with 7.25 wt.% CO_2 ("fo + 7 wt.% CO_2") and forsterite melt with 13.52 wt.% CO_2 ("fo + 14 wt.% CO_2"), and enstatite melt melt with 16.1 wt.% CO_2 ("en + 16 wt.% CO_2"). Pyrolite data is from Solomatova et al. (2019), forsterite data is from this study, and enstatite data is from Ghosh and Karki (2017). See electronic version for color representation of the figures in this book.

(Figure 16.6). When the atoms are more strongly bound in a silicate network, their diffusion rates are lower.

16.3.5. Equation of State

Solomatova et al. (2019) found that K_0 is generally positively correlated with the degree of oxidation and negatively correlated with temperature and carbon concentration; K'_0 is positively correlated with the degree of oxidation, temperature, and carbon concentration. Table 16.2 lists the equation of state parameters for a wide range of melts. Solomatova et al. find that the density difference between carbon-bearing and carbon-free pyrolite melts is larger at low pressure (where the density ratio of carbonated pyrolite to pure pyrolite ranges from 0.90 to 0.97 at 0 GPa), while above 10–20 GPa the densities converge, resulting in a density ratio of about 0.98–1. Consequently, carbon-bearing melts would be expected to be relatively less buoyant at lower-mantle pressures than at pressures of the upper mantle.

16.3.6. Diamond Formation

From a strict thermodynamical point of view, diamonds should not exist on the surface of the Earth. We find them naturally in rocks because they form at depth and are brought to the surface by uprising molten rock (magmas). Some of these diamonds coming from the deep mantle contain geochemical and mineralogical keys to the functioning of the entire silicate mantle. Hence, understanding their formation is fundamental to tracing the cycles of matter inside our planet. The formation of diamonds in Earth's deep mantle is poorly understood due to the limitations of experimental methods and our inability to access the diamond-forming depths of the mantle. Diamonds likely form in a wide range of pressure-temperature regimes and chemical environments (Cartigny et al., 2001; Kaminsky, 2012; Meyer, 1985). In the uppermost mantle, diamonds are thought to form during metamorphic reactions (Boyd & Finnerty, 1980), metasomatism (Shee et al., 1982; Sverjensky & Huang, 2015) and in magmatic processes (Meyer, 1985). It has

Table 16.2 Equation of state parameters for silicate melts with varying concentrations of carbon. We compare our results to the experimental studies on carbon-bearing peridotitic and basaltic melts (Sakamaki et al., 2011; Ghosh et al., 2007). An isothermal fourth-order Birch Murnaghan equation of state was fitted to the pressure-density data sets for the pyrolite and carbonated Mg_2SiO_4 melts. An isothermal third-order Birch Murnaghan equation of state was used to fit the pressure-volume data for Mg_2SiO_4, $MgSiO_3$ (Ghosh et al., 2017), peridotite (Sakamaki et al., 2011) and basalt (Ghosh et al., 2007).

Melt Composition	T (K)	ρ_0 (g/cm³)	K_0(GPa)	K'_0	K''_0
pyrolite[a]		2.265(2)	12.3(1)	7.8(1)	–2.4(1)
pyrolite + 3.35 wt.% CO[a]		2.19(6)	12(5)	7(3)	–2(3)
pyrolite + 5.16 wt.% CO_2[a]		2.14(1)	10.0(6)	7.6(4)	–2.5(5)
Mg_2SiO_4[b]		2.658(1)	56.3(2)	3.60(4)	—
Mg_2SiO_4 + 0.53 wt.% C[b]		2.4(1)	24(10)	6(1)	–0.5(5)
Mg_2SiO_4 + 1.92 wt.% CO_2[b]	3000	2.13(5)	10(6)	6.0(5)	–1.0(4)
Mg_2SiO_4 + 3.61 wt.% $MgCO_3$[b]		2.684(7)	39(1)	4.75(8)	–0.13(1)
$MgSiO_3$[c]		2.56(2)	18(1)	6.9(2)	—
$MgSiO_3$ + 5.2 wt.% CO_2[c]		2.43(3)	16(2)	6.5(2)	—
peridotite + 2.5 wt.% CO_2[d]		—	23(1)	7(1)	—
basalt + 5 wt.% CO_2		—	16(1)	5.2(2)	—
pyrolite[a]		2.03(4)	8(1)	8(1)	–4(3)
pyrolite + 3.35 wt.% CO[a]		1.92(4)	7(2)	6.7(9)	–2(1)
pyrolite + 5.16 wt.% CO_2[a]	4000	1.96(4)	9(2)	6.2(9)	–1(1)
pyrolite + 6.48 wt.% CO[a]		1.71(4)	3.3(6)	8.2(6)	–8(3)
pyrolite + 9.82 wt.% CO_2[a]		1.78(1)	3.8(3)	8.8(4)	–9(2)
pyrolite[a]		1.77(2)	4.9(6)	7.4(5)	–4(1)
pyrolite + 3.35 wt.% CO[a]	5000	1.56(5)	2.2(8)	9(2)	–17(15)
pyrolite + 5.16 wt.% CO_2[a]		1.56(6)	2(1)	10(3)	–19(24)

[a] Ab initio molecular dynamics calculations on pyrolite melt from Solomatova et al. (2019).
[b] Ab initio molecular dynamics calculations on Mg_2SiO_4 forsterite melt, this study.
[c] Ab initio molecular dynamics calculations on $MgSiO_3$ enstatite melt from Ghosh et al. (2017).
[d] Experimental results on peridotite melt from Sakamaki et al. (2011).
[e] Experimental results on basalt melt from Ghosh et al. (2007).

been proposed that many of the diamonds interpreted to have originated in the transition zone and lower mantle formed from subducted carbon (Burnham et al., 2015; Pal'yanov et al., 2002; Walter et al., 2011; Zedgenizov et al., 2015). However, it is likely that a fraction of super-deep diamonds, many of which may have never reached the surface, formed during the crystallization of the mantle after the moon-forming impact in the Hadean and subsequently during the Archaean and Proterozoic eons (Gurney et al., 2010; Helmstaedt et al., 2010). There have been a few computational ab initio studies examining the behavior of carbon in silicate melts with a focus on carbon coordination by oxygen (Ghosh et al., 2017; Guillot & Sator, 2011; Vuilleumier et al., 2015); however, there have been no computational studies characterizing the genesis of diamonds in pyrolitic melts.

The analysis of diamonds in metamorphic rocks provides some information on the depths at which the diamonds formed and the mechanisms by which they grew. For example, octahedral diamonds in peridotitic and eclogitic rocks displayed a spiral growth mechanism, indicating that the crystal moved freely in carbon-bearing silicate melt (Bulanova, 1995). The formation and growth of diamonds has been experimentally observed in a kimberlitic melt at 1800 **°C**–2200 **°C** and 7–7.7 GPa (Arima et al., 1993), and from dolomite+iron through carbon-iron redox reactions (Dorfman et al., 2018). However, the coordination of carbon in the melt and the mechanism of subsequent polymerization of carbon could not be determined due to limitations in experimental techniques.

Although redox reactions, such as the oxidation of methane or reduction of carbon dioxide, have been considered a necessary step for the formation of diamonds, it has been recently shown that diamonds can form from a reaction of carboxylates (e.g. acetate [CH_3COO^-]) with water at constant oxygen fugacity (Sverjensky et al., 2014; Sverjensky & Huang, 2015). In pyrolitic melts, Solomatova et al. (2019) observed various oxo-carbon species, such as C_2O_2, i.e. ethylenedione, and C_2O_4, i.e. oxalate, (Figure 16.5), suggesting that in the presence of hydrogen, the formation of diamonds from acetate is possible. These polymerized carbon chains are reminiscent of carboxylates and may be considered precursors to the formation of diamonds. This suggests a mechanism for diamond formation in pyrolitic melts

at large depths that does not necessitate the direct formation of oxygen-free carbon clusters; instead, diamond embryos on the nano scale could form through a pathway involving polymerized hydrocarbons, as described in Sverjensky et al. (2014) and Sverjensky and Huang (2015).

16.4. CONCLUSIONS

Experiments on silicate melts have demonstrated that at 1–4 GPa and 1000 °C–2000 °C, both the solubility and speciation of carbon depend most strongly on pressure and composition. Carbon solubility increases rapidly with small increases in pressure and is generally positively correlated with the concentration of CaO in the melt, while the $CO_2/(CO_2+CO_3^{2-})$ ratio is negatively correlated with pressure and is highly sensitive to the silica content, such that carbon exists almost exclusively as CO_2 in silica-rich felsic melts (e.g. rhyolite) and as CO_3^{2-} in silica-poor mafic melts (e.g. basalt). Meanwhile, molecular dynamics simulations of silicate melts at 0–140 GPa and 1400–5000 K have come to a general conclusion that there is a strong positive correlation of carbon solubility with pressure, a weak negative correlation of solubility with temperature, and a positive correlation of $CO_2/(CO_2+CO_3^{2-})$ with temperature. Simulations predict that the concentration of CO_2 sharply decreases at the expense of CO_3^{2-} with increasing pressure between 0 and 5 GPa, in agreement with experimental observations; between 10 and 140 GPa, pressures above what has been achieved by most experiments on carbonated silicate melts, CO_4^{4-} species appear and their concentration increases with increasing pressure at the expense of $CO_2+CO_3^{2-}$.

Here we also demonstrate a need for high-pressure high-temperature experiments on carbonated multicomponent silicate melts to confirm the computationally predicted carbon-carbon polymerization, carbon-silicon bonding, and carbon-iron complexes. Ab initio computational studies on CO_2-H_2O-bearing silicate melts would help understand the effect of water on carbon's speciation and solubility. The detailed effect of composition and polymerization in complex silicate melts needs to be determined both experimentally and computationally, to thoroughly understand the speciation and solubility of carbon in the interior of the Earth. Finally, to constrain the carbon concentration of Earth's interior, it is crucial to determine the fraction of carbon that was retained in the planet after the Giant Impact via calculations on the volatility of carbon in pyrolitic-type melt and of partitioning between the molten magma ocean and molten core.

ACKNOWLEDGMENTS

REFERENCES

Arima, M., Nakayama, K., Akaishi, M., Yamaoka, S., & Kanda, H. (1993). Crystallization of diamond from a silicate melt of kimberlite composition in high-pressure and high-temperature experiments. *Geology*, *21*(11), 968. https://doi.org/10.1130/0091-7613(1993)021<0968:CODFAS>2.3.CO;2

Behrens, H., Misiti, V., Freda, C., Vetere, F., Botcharnikov, R. E., & Scarlato, P. (2009). Solubility of H_2O and CO_2 in ultra-potassic melts at 1200 and 1250 °C and pressure from 50 to 500 MPa. *American Mineralogist*, *94*(1), 105–120. https://doi.org/10.2138/am.2009.2796

Behrens, H., & Nowak, M. (2003). Quantification of H_2O speciation in silicate glasses and melts by IR spectroscopy: In situ versus quench techniques. *Phase Transitions*, *76*(1–2), 45–61. https://doi.org/10.1080/0141159031000076048

Behrens, H., Zhang, Y., & Xu, Z. (2004). H_2O diffusion in dacitic and andesitic melts. *Geochimica et Cosmochimica Acta*, *68*(24), 5139–5150. https://doi.org/10.1016/j.gca.2004.07.008

Blank, J. G. (1993). An experimental investigation of the behavior of carbon dioxide in rhyolitic melt (PhD thesis). California Institute of Technology. Retrieved from http://resolver.caltech.edu/CaltechETD:etd-05302007-075656

Blank, J. G., & Brooker, R. A. (1994). Experimental studies of carbon dioxide in silicate melts: Solubility, speciation, and stable carbon isotope behavior. *Reviews in Mineralogy and Geochemistry*, *30*, 157–186.

Blank, J. G., Stolper, E. M., & Carroll, M. R. (1993). Solubilities of carbon dioxide and water in rhyolitic melt at 850 °C and 750 bars. *Earth and Planetary Science Letters*, *119*(1–2), 27–36. https://doi.org/10.1016/0012-821X(93)90004-S

Botcharnikov, R. E., Behrens, H., & Holtz, F. (2006). Solubility and speciation of C–O–H fluids in andesitic melt at T= 1100–1300 C and P= 200 and 500 MPa. *Chemical Geology*, *229*(1–3), 125–143. https://doi.org/10.1016/j.chemgeo.2006.01.016

Botcharnikov, R. E., Koepke, J., Holtz, F., McCammon, C., & Wilke, M. (2005). The effect of water activity on the oxidation and structural state of Fe in a ferro-basaltic melt. *Geochimica et Cosmochimica Acta*, *69*(21), 5071–5085. https://doi.org/10.1016/j.gca.2005.04.023

Botcharnikov, Roman E., Holtz, F., & Behrens, H. (2007). The effect of CO_2 on the solubility of H_2O-Cl fluids in andesitic

melt. *European Journal of Mineralogy*, *19*(5), 671–680. https://doi.org/10.1127/0935-1221/2007/0019-1752

Boyd, F. R., & Finnerty, A. A. (1980). Conditions of origin of natural diamonds of peridotite affinity. *Journal of Geophysical Research: Solid Earth*, *85*(B12), 6911–6918. https://doi.org/10.1029/JB085iB12p06911

Brenker, F., Vollmer, C., Vincze, L., Vekemans, B., Szymanski, A., Janssens, K., et al. (2006). CO_2-recycling to the deep convecting mantle. *Geochimica et Cosmochimica Acta*, *70*(18), 66.

Brey, G. (1976). CO_2 solubility and solubility mechanisms in silicate melts at high pressures. *Contributions to Mineralogy and Petrology*, *57*(2), 215–221. https://doi.org/10.1007/BF00405226

Brey, G. P., & Green, D. H. (1976). Solubility of CO_2 in olivine melilitite at high pressures and role of CO_2 in the earth's upper mantle. *Contributions to Mineralogy and Petrology*, *55*(2), 217–230. https://doi.org/10.1007/BF00372228

Brooker, R. A., Kohn, S. C., Holloway, J. R., & McMillan, P. F. (2001a). Structural controls on the solubility of CO_2 in silicate melts: Part I. Bulk solubility data. *Chemical Geology*, *174*(1), 225–239. https://doi.org/10.1016/S0009-2541(00)00353-3

Brooker, R. A., Kohn, S. C., Holloway, J. R., & McMillan, P. F. (2001b). Structural controls on the solubility of CO_2 in silicate melts: Part II. IR characteristics of carbonate groups in silicate glasses. *Chemical Geology*, *174*(1), 241–254. https://doi.org/10.1016/S0009-2541(00)00318-1

Brooker, R. A., Kohn, S. C., Holloway, J. R., McMillan, P. F., & Carroll, M. R. (1999). Solubility, speciation and dissolution mechanisms for CO_2 in melts on the NaAlO2–SiO2 join. *Geochimica et Cosmochimica Acta*, *63*(21), 3549–3565. https://doi.org/10.1016/S0016-7037(99)00196-9

Bulanova, G. P. (1995). The formation of diamond. *Journal of Geochemical Exploration*, *53*(1), 1–23. https://doi.org/10.1016/0375-6742(94)00016-5

Burnham, A. D., Thomson, A. R., Bulanova, G. P., Kohn, S. C., Smith, C. B., & Walter, M. J. (2015). Stable isotope evidence for crustal recycling as recorded by superdeep diamonds. *Earth and Planetary Science Letters*, *432*, 374–380. https://doi.org/10.1016/j.epsl.2015.10.023

Cartigny, P., Harris, J. W., & Javoy, M. (2001). Diamond genesis, mantle fractionations and mantle nitrogen content: a study of δ13C–N concentrations in diamonds. *Earth and Planetary Science Letters*, *185*(1), 85–98. https://doi.org/10.1016/S0012-821X(00)00357-5

Dixon, J. E. (1997). Degassing of alkalic basalts. *American Mineralogist*, *82*(3–4), 368–378. https://doi.org/10.2138/am-1997-3-415

Dorfman, S. M., Badro, J., Nabiei, F., Prakapenka, V. B., Cantoni, M., & Gillet, P. (2018). Carbonate stability in the reduced lower mantle. *Earth and Planetary Science Letters*, *489*, 84–91. https://doi.org/10.1016/j.epsl.2018.02.035

Duan, X. (2014). A general model for predicting the solubility behavior of H_2O–CO_2 fluids in silicate melts over a wide range of pressure, temperature and compositions. *Geochimica et Cosmochimica Acta*, *125*, 582–609. https://doi.org/10.1016/j.gca.2013.10.018

Eggler, D. H. (1987). Discussion of recent papers on carbonated peridotite, bearing on mantle metasomatism and magmatism: An alternative. *Earth and Planetary Science Letters*, *82*(3), 398–400. https://doi.org/10.1016/0012-821X(87)90214-7

Eitel, W., & Weyl, W. (1932). Residuals in the melting of commercial glasses. *Journal of the American Ceramic Society*, *15*(3), 159–166. https://doi.org/10.1111/j.1151-2916.1932.tb13916.x

Fine, G., & Stolper, E. (1985). The speciation of carbon dioxide in sodium aluminosilicate glasses. *Contributions to Mineralogy and Petrology*, *91*(2), 105–121. https://doi.org/10.1007/BF00377759

Fine, G., & Stolper, E. (1986). Dissolved carbon dioxide in basaltic glasses: Concentrations and speciation. *Earth and Planetary Science Letters*, *76*(3–4), 263–278. https://doi.org/10.1016/0012-821X(86)90078-6

Fogel, R. A., & Rutherford, M. J. (1990). The solubility of carbon dioxide in rhyolitic melts: A quantitative FTIR study. *American Mineralogist*, *75*(11–12), 1311–1326.

Ghosh, D. B., Bajgain, S. K., Mookherjee, M., & Karki, B. B. (2017). Carbon-bearing silicate melt at deep mantle conditions. *Scientific Reports*, *7*(1). https://doi.org/10.1038/s41598-017-00918-x

Ghosh, D. B., & Karki, B. B. (2017). Transport properties of carbonated silicate melt at high pressure. *Science Advances*, *3*(12), e1701840. https://doi.org/10.1126/sciadv.1701840

Ghosh, S., Ohtani, E., Litasov, K., Suzuki, A., & Sakamaki, T. (2007). Stability of carbonated magmas at the base of the Earth's upper mantle. *Geophysical Research Letters*, *34*(22). https://doi.org/10.1029/2007GL031349

Guillot, B., & Sator, N. (2011). Carbon dioxide in silicate melts: A molecular dynamics simulation study. *Geochimica et Cosmochimica Acta*, *75*(7), 1829–1857. https://doi.org/10.1016/j.gca.2011.01.004

Gurney, J. J., Helmstaedt, H. H., Richardson, S. H., & Shirey, S. B. (2010). Diamonds through time. *Economic Geology*, *105*(3), 689–712. https://doi.org/10.2113/gsecongeo.105.3.689

Gygi, F. (2018). Qbox: A large-scale parallel implementation of first-principles molecular dynamics. http://www.qboxcode.org/

Hammouda, T. (2003). High-pressure melting of carbonated eclogite and experimental constraints on carbon recycling and storage in the mantle. *Earth and Planetary Science Letters*, *214*(1–2), 357–368. https://doi.org/10.1016/S0012-821X(03)00361-3

Helmstaedt, H. H., Gurney, J. J., & Richardson, S. H. (2010). Ages of cratonic diamond and lithosphere evolution: Constraints on precambrian tectonics and diamond exploration. *The Canadian Mineralogist*, *48*(6), 1385–1408. https://doi.org/10.3749/canmin.48.5.1385

Holloway, J. R. (1976). Fluids in the evolution of granitic magmas: Consequences of finite CO_2 solubility. *GSA Bulletin*, *87*(10), 1513–1518. https://doi.org/10.1130/0016-7606(1976)87<1513:FITEOG>2.0.CO;2

Holloway, J. R., & Blank, J. G. (1994). Application of experimental results to C-O-H species in natural melts. *Reviews in Mineralogy and Geochemistry*, *30*(1), 187–230.

Iacono-Marziano, G., Morizet, Y., Le Trong, E., & Gaillard, F. (2012). New experimental data and semi-empirical parameterization of H_2O–CO_2 solubility in mafic melts. *Geochimica et Cosmochimica Acta*, *97*, 1–23. https://doi.org/10.1016/j.gca.2012.08.035

Isshiki, M., Irifune, T., Hirose, K., Ono, S., Ohishi, Y., Watanuki, T., et al. (2004). Stability of magnesite and its high-pressure form in the lowermost mantle. *Nature*, *427*(6969), 60–63. https://doi.org/10.1038/nature02181

Jakobsson, S. (1997). Solubility of water and carbon dioxide in an icelandite at 1400 °C and 10 kilobars. *Contributions to Mineralogy and Petrology*, *127*(1), 129–135. https://doi.org/10.1007/s004100050270

Jendrzejewski, N., Trull, T. W., Pineau, F., & Javoy, M. (1997). Carbon solubility in mid-ocean ridge basaltic melt at low pressures (250–1950 bar). *Chemical Geology*, *138*(1–2), 81–92. https://doi.org/10.1016/S0009-2541(96)00176-3

Kadik, A. (2004). Formation of carbon and hydrogen species in magmas at low oxygen fugacity. *Journal of Petrology*, *45*(7), 1297–1310. https://doi.org/10.1093/petrology/egh007

Kaminsky, F. (2012). Mineralogy of the lower mantle: A review of 'super-deep' mineral inclusions in diamond. *Earth-Science Reviews*, *110*(1), 127–147. https://doi.org/10.1016/j.earscirev.2011.10.005

Keppler, H., Wiedenbeck, M., & Shcheka, S. S. (2003). Carbon solubility in olivine and the mode of carbon storage in the Earth's mantle. *Nature*, *424*(6947), 414–416. https://doi.org/10.1038/nature01828

King, P. L., & Holloway, J. R. (2002). CO_2 solubility and speciation in intermediate (andesitic) melts: The role of H_2O and composition. *Geochimica et Cosmochimica Acta*, *66*(9), 1627–1640. https://doi.org/10.1016/S0016-7037(01)00872-9

Konschak, A., & Keppler, H. (2014). The speciation of carbon dioxide in silicate melts. *Contributions to Mineralogy and Petrology*, *167*(5). https://doi.org/10.1007/s00410-014-0998-2

Lesne, P., Scaillet, B., Pichavant, M., & Beny, J.-M. (2011). The carbon dioxide solubility in alkali basalts: An experimental study. *Contributions to Mineralogy and Petrology*, *162*(1), 153–168. https://doi.org/10.1007/s00410-010-0585-0

Mao, Z., Armentrout, M., Rainey, E., Manning, C. E., Dera, P., Prakapenka, V. B., & Kavner, A. (2011). Dolomite III: A new candidate lower mantle carbonate: high-pressure phase of Fe-dolomite. *Geophysical Research Letters*, *38*(22), n/a-n/a. https://doi.org/10.1029/2011GL049519

Mattey, D. P. (1991). Carbon dioxide solubility and carbon isotope fractionation in basaltic melt. *Geochimica et Cosmochimica Acta*, *55*(11), 3467–3473. https://doi.org/10.1016/0016-7037(91)90508-3

McDonough, W. F. (2003). Compositional model for the Earth's core. *Treatise on Geochemistry*, 547–568.

Merlini, M., Crichton, W. A., Hanfland, M., Gemmi, M., Muller, H., Kupenko, I., & Dubrovinsky, L. (2012). Structures of dolomite at ultrahigh pressure and their influence on the deep carbon cycle. *Proceedings of the National Academy of Sciences*, *109*(34), 13509–13514. https://doi.org/10.1073/pnas.1201336109

Meyer, H. O. A. (1985). Genesis of diamond: A mantle saga. *American Mineralogist*, *70*(3–4), 344–355.

Mookherjee, M., Nakajima, Y., Steinle-Neumann, G., Glazyrin, K., Wu, X., Dubrovinsky, L., et al. (2011). High-pressure behavior of iron carbide (Fe_7C_3) at inner core conditions. *Journal of Geophysical Research: Solid Earth*, *116*(B4). https://doi.org/10.1029/2010JB007819

Moore, G. (2008). Interpreting H_2O and CO_2 contents in melt inclusions: Constraints from solubility experiments and modeling. *Reviews in Mineralogy and Geochemistry*, *69*(1), 333–362. https://doi.org/10.2138/rmg.2008.69.9

Morizet, Y., Paris, M., Gaillard, F., & Scaillet, B. (2010). C–O–H fluid solubility in haplobasalt under reducing conditions: An experimental study. *Chemical Geology*, *279*(1), 1–16. https://doi.org/10.1016/j.chemgeo.2010.09.011

Mörner, N.-A., & Etiope, G. (2002). Carbon degassing from the lithosphere. *Global and Planetary Change*, *33*(1), 185–203. https://doi.org/10.1016/S0921-8181(02)00070-X

Moussallam, Y., Morizet, Y., & Gaillard, F. (2016). H_2O–CO_2 solubility in low SiO2-melts and the unique mode of kimberlite degassing and emplacement. *Earth and Planetary Science Letters*, *447*, 151–160. https://doi.org/10.1016/j.epsl.2016.04.037

Mysen, B. O. (1976). The role of volatiles in silicate melts: Solubility of carbon dioxide and water in feldspar, pyroxene, and feldspathoid melts to 30 kb and 1625 degrees C. *American Journal of Science*, *276*(8), 969–996.

Mysen, B. O., Fogel, M. L., Morrill, P. L., & Cody, G. D. (2009). Solution behavior of reduced COH volatiles in silicate melts at high pressure and temperature. *Geochimica et Cosmochimica Acta*, *73*(6), 1696–1710. https://doi.org/10.1016/j.gca.2008.12.016

Ni, H., & Keppler, H. (2013). Carbon in silicate melts. *Reviews in Mineralogy and Geochemistry*, *75*(1), 251–287. https://doi.org/10.2138/rmg.2013.75.9

Oganov, A. R., Ono, S., Ma, Y., Glass, C. W., & Garcia, A. (2008). Novel high-pressure structures of $MgCO_3$, $CaCO_3$ and CO_2 and their role in Earth's lower mantle. *Earth and Planetary Science Letters*, *273*(1–2), 38–47. https://doi.org/10.1016/j.epsl.2008.06.005

Ono, S. (2005). Post-aragonite phase transformation in CaCO3 at 40 GPa. *American Mineralogist*, *90*(4), 667–671. https://doi.org/10.2138/am.2005.1610

Pal'yanov, Y. N., Sokol, A. G., Borzdov, Y. M., Khokhryakov, A. F., & Sobolev, N. V. (2002). Diamond formation through carbonate-silicate interaction. *American Mineralogist*, *87*(7), 1009–1013. https://doi.org/10.2138/am-2002-0726

Pan, V., Holloway, J. R., & Hervig, R. L. (1991). The pressure and temperature dependence of carbon dioxide solubility in tholeiitic basalt melts. *Geochimica et Cosmochimica Acta*, *55*(6), 1587–1595. https://doi.org/10.1016/0016-7037(91)90130-W

Panero, W. R., & Kabbes, J. E. (2008). Mantle-wide sequestration of carbon in silicates and the structure of magnesite II. *Geophysical Research Letters*, *35*(14). https://doi.org/10.1029/2008GL034442

Papale, P., Moretti, R., & Barbato, D. (2006). The compositional dependence of the saturation surface of H_2O+CO_2 fluids in silicate melts. *Chemical Geology*, *229*(1), 78–95. https://doi.org/10.1016/j.chemgeo.2006.01.013

Pawley, A. R., Holloway, J. R., & McMillan, P. F. (1992). The effect of oxygen fugacity on the solubility of carbon-oxygen fluids in basaltic melt. *Earth and Planetary Science Letters*, *110*(1), 213–225. https://doi.org/10.1016/0012-821X(92)90049-2

Pearce, M. L. (1964). Solubility of carbon dioxide and variation of oxygen ion activity in soda-silica melts. *Journal of the American Ceramic Society*, *47*(7), 342–347. https://doi.org/10.1111/j.1151-2916.1964.tb12998.x

Pearson, V. K., Sephton, M. A., Franchi, I. A., Gibson, J. M., & Gilmour, I. (2006). Carbon and nitrogen in carbonaceous chondrites: Elemental abundances and stable isotopic compositions. *Meteoritics & Planetary Science*, *41*(12), 1899–1918. https://doi.org/10.1111/j.1945-5100.2006.tb00459.x

Sakamaki, T., Ohtani, E., Urakawa, S., Terasaki, H., & Katayama, Y. (2011). Density of carbonated peridotite magma at high pressure using an X-ray absorption method. *American Mineralogist*, *96*(4), 553–557. https://doi.org/10.2138/am.2011.3577

Sen, S., Widgeon, S. J., Navrotsky, A., Mera, G., Tavakoli, A., Ionescu, E., & Riedel, R. (2013). Carbon substitution for oxygen in silicates in planetary interiors. *Proceedings of the National Academy of Sciences*, *110*(40), 15904–15907. https://doi.org/10.1073/pnas.1312771110

Shcheka, S. S., Wiedenbeck, M., Frost, D. J., & Keppler, H. (2006). Carbon solubility in mantle minerals. *Earth and Planetary Science Letters*, *245*(3), 730–742. https://doi.org/10.1016/j.epsl.2006.03.036

Shee, S. R., Gurney, J. J., & Robinson, D. N. (1982). Two diamond-bearing peridotite xenoliths from the finsch kimberlite, South Africa. *Contributions to Mineralogy and Petrology*, *81*(2), 79–87. https://doi.org/10.1007/BF00372045

Shishkina, T. A., Botcharnikov, R. E., Holtz, F., Almeev, R. R., Jazwa, A. M., & Jakubiak, A. A. (2014). Compositional and pressure effects on the solubility of H_2O and CO_2 in mafic melts. *Chemical Geology*, *388*, 112–129. https://doi.org/10.1016/j.chemgeo.2014.09.001

Shishkina, T. A., Botcharnikov, R. E., Holtz, F., Almeev, R. R., & Portnyagin, M. V. (2010). Solubility of H_2O- and CO_2-bearing fluids in tholeiitic basalts at pressures up to 500 MPa. *Chemical Geology*, *277*(1), 115–125. https://doi.org/10.1016/j.chemgeo.2010.07.014

Sobolev, N. V., & Shatsky, V. S. (1990). Diamond inclusions in garnets from metamorphic rocks: A new environment for diamond formation. *Nature*, *343*(6260), 742–746. https://doi.org/10.1038/343742a0

Solomatova, N. V., & Asimow, P. D. (2017). Ab initio study of the structure and stability of $CaMg(CO_3)_2$ at high pressure. *American Mineralogist*, *102*(1), 210–215. https://doi.org/10.2138/am-2017-5830

Solomatova, N. V., Caracas, R., & Manning, M. E. (2019). Carbon sequestration during core formation implied by complex carbon polymerization. *Nature Communications*, *10*(1), 789. https://doi.org/10.1038/s41467-019-08742-9

Stanley, B. D., Hirschmann, M. M., & Withers, A. C. (2011). CO_2 solubility in Martian basalts and Martian atmospheric evolution. *Geochimica et Cosmochimica Acta*, *75*(20), 5987–6003. https://doi.org/10.1016/j.gca.2011.07.027

Stolper, E., Fine, G., Johnson, T., & Newman, S. (1987). Solubility of carbon dioxide in albitic melt. *American Mineralogist*, *72*(11–12), 1071–1085.

Stolper, E., & Holloway, J. R. (1988). Experimental determination of the solubility of carbon dioxide in molten basalt at low pressure. *Earth and Planetary Science Letters*, *87*(4), 397–408. https://doi.org/10.1016/0012-821X(88)90004-0

Sverjensky, D. A., & Huang, F. (2015). Diamond formation due to a pH drop during fluid–rock interactions. *Nature Communications*, *6*(1). https://doi.org/10.1038/ncomms9702

Sverjensky, D. A., Stagno, V., & Huang, F. (2014). Important role for organic carbon in subduction-zone fluids in the deep carbon cycle. *Nature Geoscience*, *7*(12), 909–913. https://doi.org/10.1038/ngeo2291

Tamic, N., Behrens, H., & Holtz, F. (2001). The solubility of H_2O and CO_2 in rhyolitic melts in equilibrium with a mixed CO_2–H_2O fluid phase. *Chemical Geology*, *174*(1), 333–347. https://doi.org/10.1016/S0009-2541(00)00324-7

Tamic, N., Behrens, H., & Holtz, F. (2001). The solubility of H_2O and CO_2 in rhyolitic melts in equilibrium with a mixed CO_2–H_2O fluid phase. *Chemical Geology*, *174*(1), 333–347. https://doi.org/10.1016/S0009-2541(00)00324-7

Thibault, Y., & Holloway, J. R. (1994). Solubility of CO_2 in a Ca-rich leucitite: Effects of pressure, temperature, and oxygen fugacity. *Contributions to Mineralogy and Petrology*, *116*(1), 216–224. https://doi.org/10.1007/BF00310701

Thomsen, T. B., & Schmidt, M. W. (2008). Melting of carbonated pelites at 2.5–5.0 GPa, silicate–carbonatite liquid immiscibility, and potassium–carbon metasomatism of the mantle. *Earth and Planetary Science Letters*, *267*(1), 17–31. https://doi.org/10.1016/j.epsl.2007.11.027

Vetere, F., Botcharnikov, R. E., Holtz, F., Behrens, H., & De Rosa, R. (2011). Solubility of H_2O and CO_2 in shoshonitic melts at 1250 °C and pressures from 50 to 400MPa: Implications for Campi Flegrei magmatic systems. *Journal of Volcanology and Geothermal Research*, *202*(3), 251–261. https://doi.org/10.1016/j.jvolgeores.2011.03.002

Vetere, F., Holtz, F., Behrens, H., Botcharnikov, R. E., & Fanara, S. (2014). The effect of alkalis and polymerization on the solubility of H_2O and CO_2 in alkali-rich silicate melts. *Contributions to Mineralogy and Petrology*, *167*(5), 1014. https://doi.org/10.1007/s00410-014-1014-6

Vuilleumier, R., Seitsonen, A. P., Sator, N., & Guillot, B. (2015). Carbon dioxide in silicate melts at upper mantle conditions: Insights from atomistic simulations. *Chemical Geology*, *418*, 77–88. https://doi.org/10.1016/j.chemgeo.2015.02.027

Walter, M. J., Kohn, S. C., Araujo, D., Bulanova, G. P., Smith, C. B., Gaillou, E., et al. (2011). Deep mantle cycling of oceanic crust: Evidence from diamonds and their mineral inclusions. *Science*, *334*(6052), 54–57. https://doi.org/10.1126/science.1209300

Webster, J. D., & Botcharnikov, R. E. (2011). Distribution of sulfur between melt and fluid in S-O-H-C-Cl-bearing magmatic systems at shallow crustal pressures and temperatures. *Reviews in Mineralogy and Geochemistry*, *73*(1), 247–283. https://doi.org/10.2138/rmg.2011.73.9

Wood, B. J. (1993). Carbon in the core. *Earth and Planetary Science Letters*, *117*(3), 593–607. https://doi.org/10.1016/0012-821X(93)90105-I

Wyllie, P. J., Baker, M. B., & White, B. S. (1990). Experimental boundaries for the origin and evolution of carbonatites. *Lithos*, *26*(1), 3–19. https://doi.org/10.1016/0024-4937(90)90037-2

Zedgenizov, D. A., Shatsky, V. S., Panin, A. V., Evtushenko, O. V., Ragozin, A. L., & Kagi, H. (2015). Evidence for phase transitions in mineral inclusions in superdeep diamonds of the Sao Luiz deposit (Brazil). *Russian Geology and Geophysics*, *56*(1), 296–305. https://doi.org/10.1016/j.rgg.2015.01.021